

Direct numerical simulation of the Ekman layer: A step in Reynolds number, and cautious support for a log law with a shifted origin

Philippe R. Spalart,¹ Gary N. Coleman,² and Roderick Johnstone³

¹Boeing Commercial Airplanes, P.O. Box 3707, Seattle, Washington 98124, USA

²School of Engineering Sciences, University of Southampton, Southampton SO17 1BJ, United Kingdom

³STFC Daresbury Laboratory, Daresbury, Warrington WA4 4AD, United Kingdom

(Received 18 December 2007; accepted 6 May 2008; published online 31 October 2008)

Results at Ekman Reynolds numbers Re ranging from 1000 to 2828 expand the direct numerical simulation (DNS) contribution to the theory of wall-bounded turbulence. An established spectral method is used, with rules for domain size and grid resolution at each Reynolds number derived from the theory. The Re increase is made possible by better computers and by optimizing the grid in relation to the wall shear-stress direction. The boundary-layer thickness in wall units δ^+ varies here by a factor of about 5.3, and reaches values near 5000, or 22 times the minimum at which turbulence has been sustained. An equivalent channel Reynolds number, based on the pressure gradient in wall units, would reach about $Re_\tau=1250$. The principal goal of the analysis, the impartial identification of a log law, is summarized in the local “Karman measure” $d(\ln z^+)/dU^+$. The outcome differs from that for Hoyas and Jiménez [Phys. Fluids **18**, 011702 (2006)] and for Hu *et al.* [AIAA J. **44**, 1541 (2006)] in channel-flow DNS at similar Reynolds numbers, for reasons unknown: Here, the law of the wall is gradually established up to a z^+ around 400, with little statistical scatter. To leading order, it is consistent with the experiments of Österlund *et al.* [Phys. Fluids **12**, 1 (2000)] in boundary layers. With the traditional expression, a logarithmic law is not present, in that the Karman measure drifts from about 0.41 at $z^+\approx 70$ to the 0.37–0.38 range for $z^+\approx 500$, with $Re=2828$. However, if a virtual origin is introduced with a shift of $a^+=7.5$ wall units, the data support a long logarithmic layer with $\kappa=0.38$ a good fit to $d(\ln[z^++a^+])/dU^+$. A determination of the Karman constant from the variation of the skin-friction coefficients with Reynolds numbers also yields values near 0.38. The uncertainty is about ± 0.01 . These values are close to the boundary-layer experiments, but well below the accepted range of [0.40,0.41] and the experimental pipe-flow results near 0.42. The virtual-origin concept is also controversial, although nonessential at transportation or atmospheric Reynolds numbers. Yet, this series may reflect some success in verifying the law of the wall and investigating the logarithmic law by DNS, redundantly and with tools more impartial than the visual fit of a straight line to a velocity profile. © 2008 American Institute of Physics. [DOI: 10.1063/1.3005858]

I. INTRODUCTION AND APPROACH

The turbulent Ekman layer is a statistically stationary pressure-driven three-dimensional boundary layer (3DBL) obtained in a rotating system, induced by the viscous effect upon a flow that far from the boundary is in geostrophic balance. It thus involves a three-way equilibrium between the horizontal (i.e., parallel to the no-slip boundary) mean pressure gradient, the Coriolis acceleration, and the vertical (normal to the boundary) gradient of Reynolds stress. As a result, both the magnitude and direction of the mean velocity change with distance from the surface (see Fig. 1). However at the higher Reynolds numbers, the direction is essentially unchanged for $\frac{2}{3}$ of the velocity rise, so that 3D effects are remote in wall units, and this flow is as legitimate as a two-dimensional channel or boundary layer as a case study of wall-bounded turbulence theory. The Ekman layer is a model for engineering 3DBLs such as those found on swept-wing aircraft, as well as an idealization of the Earth’s planetary boundary layer. It has the practical advantage that the DNS is statistically homogeneous in both wall-parallel directions, and time.

We simulate this flow at Reynolds number $Re=GD/\nu$ ranging from 1000 to 2828, where G is the geostrophic wind speed, ν the kinematic viscosity, $D=\sqrt{2\nu/f}$ the viscous boundary-layer depth, and $f=2\Omega_V$ the Coriolis parameter. We limit our attention to the case with no horizontal rotation, $\Omega_H=0$. It will be seen that the boundary-layer thickness expressed in wall units, δ^+ , scales approximately like $Re^{1.6}$ in the present range (Sec. II B presents the general formula). This study complements earlier Ekman DNS at $Re=400$,^{1,2} 500,¹ and 1000,³ as well as current efforts toward high-Reynolds number in channel flow.^{4,5} Our ambition is to quantify as finely as is feasible Reynolds-number effects over the 400–2828 range, with an eye toward generalizing to Re ranges of interest to the engineering and especially meteorology communities.

The computations were conducted using a fully spectral Fourier/Jacobi⁶ MPI-based code on up to 204 processors of the UK HPCx IBM p690+ cluster. (The previous DNS summarized in Table I used a serial version of this algorithm on various vector machines.) Numerical parameters are chosen such that for each of the $Re=1000, 1414, 2000,$ and 2828

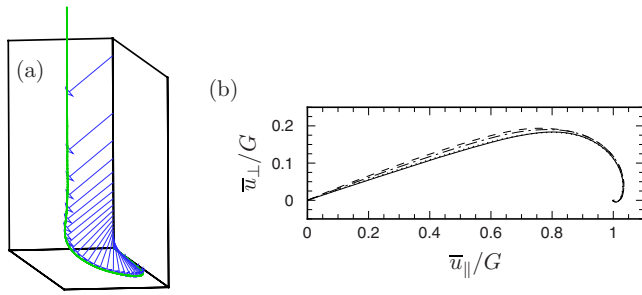


FIG. 1. (Color online) (a) Schematic of Ekman spiral (here laminar). (b) Mean velocity hodograph: (----) Re=1000; (— · —) Re=1414; (·····) Re=2000; (—) Re=2828.

runs, the periodic lateral domain has the same size in units of the outer-layer length scale u_* / f (where u_* is the surface friction velocity), namely, $\Lambda = \Lambda_x = \Lambda_y \approx 2.0 u_* / f$. This length scale was accepted as determining the outer region as early as 1967 by Csanady, and previous DNS results over a fair range of Reynolds number have been fully consistent with the idea that it determines the size of the largest outer-layer eddies. The angle φ_G between the freestream geostrophic wind and the x axis is set based on similarity theory (Ref. 7 and Sec. II B), so that the x axis is close to parallel to the surface shear stress (see Table I). The difference between φ_G and the actual surface-stress orientation α_0 given by the DNS is shown in Table I. Because $\cos(\varphi_G - \alpha_0) \approx 1$ at each Re, the near-wall resolution of 21 and 7 wall units in x and y used here corresponds, respectively, to the directions along and across the direction of the mean surface shear. These two values were validated by Spalart⁸ and others. The benefit of aligning the Cartesian grid with the surface stress can be seen in Table I, by comparing the number of grid points used for the earlier Re=400, 500, and 1000 cases (for which the x -axis was parallel to \mathbf{G}) with the number needed here. This strategy allowed us to increase significantly the largest Re we were able to consider.

The z direction is vertical. The length scale ℓ_z used in the exponential mapping is fixed at $\ell_z = 0.25 u_* / f$ for each case,⁹ again conforming to the accepted outer length scale, and the collocation points distributed such that the first ten fall at or below $z^+ = z u_* / \nu = 10$. To avoid aliasing, the number of collocation (quadrature) points (N_x, N_y, N_z) is 50% greater than the corresponding number of Fourier or Jacobi expansion coefficients. At Re=2000, $(N_x, N_y, N_z) = (420, 1260, 151)$,

while for Re=2828 a $(N_x, N_y, N_z) = (768, 2304, 204)$ grid is required.

The suitability of the numerical parameters is revealed by the streamwise and lateral energy spectra in Fig. 2. The high wavenumber behavior of both components, at both inner- and outer-layer elevations, reflects the quality of the small-scale resolution. The slopes -1 and $-5/3$ are drawn for reference, and some agreement with them is arguable in some regions. Just like for the velocity profile, a well-grounded discussion of this will require seeking plateaus in derivatives (here, with precisely known target values), rather than rectilinear behavior of the function itself. The small-wavenumber variation is of more concern. Although exaggerated in this log-log scaling, the negative slope at the smallest (nonzero) wavenumbers suggests that the very largest scales supported by the DNS are not completely unaffected by the finite horizontal size Λ of the domain. This is a recurrent difficulty of boundary-layer simulations.⁸ An alternate check of the domain size is given in Fig. 3, where contours at representative elevations of two-point velocity correlations in the horizontal x - y plane, $R_{ii}(\mathbf{r}, z) = \overline{u'_i(\mathbf{x})u'_i(\mathbf{x}+\mathbf{r})} / q^2(z)$ [where $\mathbf{r} = (r_x, r_y)$ is the horizontal separation distance and $q^2 = \overline{u'_j(\mathbf{x})u'_j(\mathbf{x})}$], are superimposed upon the horizontal domain; the subscript ii denotes summation over the three velocity components. These imply that all but the very largest naturally occurring scales are included in the simulation (the chain-dot curve corresponds to $R_{ii}=0$; the largest solid contour at each elevation is $R_{ii}=0.1$). The change in direction of the footprint motivates the use of a square x - y domain. The effect of the “missing” scales on low-order statistics has been shown to be very weak in earlier domain-size tests (e.g., comparing Cases C90 and D90 of Ref. 1, and the previous¹ and present “Case A90” results). Quantities such as the drag coefficient and boundary-layer depth are therefore expected to differ only very slightly from the infinite-domain ideal.

Perspective on the domain size may benefit from the following remark. When DNS is used to address issues of universal behavior of the inner layer toward the high-Re regime, the strategy is to consider cases at various Reynolds numbers with the same (in size, intensity, and number) large dominant eddies in the upper layer, but new generations of increasingly small and numerous near-surface eddies. This leads to the requirement of maintaining, as Re increases, the horizontal size of the domain at a fixed multiple of u_* / f

TABLE I. Run parameters.

Source	Re	φ_G (deg)	$\varphi_G - \alpha_0$ (deg)	$f\Lambda / u_*$	N_x	N_y	Δx^+	Δy^+	$f\ell_z / u_*$	N_z	z_{10}^+	Δr^+
Refs. 1 and 2 (1996)	400	0	-27.81	8.01	384	384	7.2	7.2	0.250	45	9.2	0.300
Ref. 1 (1990)	500	0	-25.35	2.10	128	128	8.0	8.0	0.262	50	11.0	0.419
Ref. 3 (1999)	1000	0	-19.00	1.86	384	384	7.0	7.0	0.232	85	9.9	0.266
New	1000	19.00	-0.36	2.02	140	420	20.6	6.9	0.252	88	9.9	0.254
New	1414	18.00	+0.13	2.01	256	768	19.4	6.5	0.252	115	9.9	0.211
New	2000	16.00	-0.36	1.99	420	1260	20.7	6.9	0.249	151	10.05	0.165
New	2828	15.12	-0.45	2.00	768	2304	19.9	6.6	0.250	204	9.7	0.166

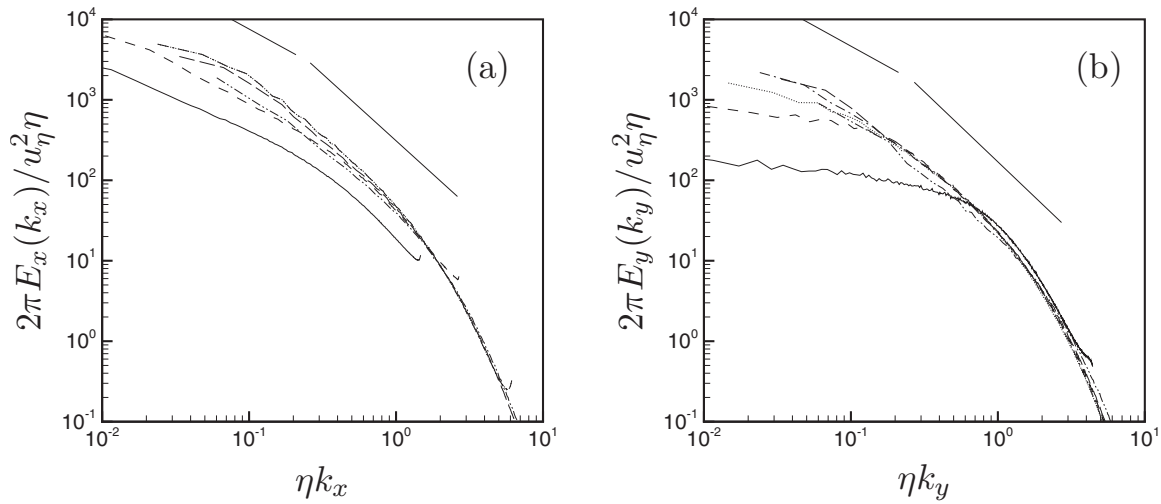


FIG. 2. One-dimensional turbulent kinetic energy spectra in (a) streamwise and (b) lateral directions for $Re=2828$ DNS: —, $z/\delta^*=0.003(z^+=23)$; (----) $z/\delta^*=0.03(z^+=226)$; (·····) $z/\delta^*=0.10(z^+=760)$; (— · —) $z/\delta^*=0.30(z^+=2277)$; (---) $z/\delta^*=0.46(z^+=3477)$; (— · · —) $z/\delta^*=0.78(z^+=5921)$. Streamwise k_x and lateral k_y wavenumbers and spectra normalized by Kolmogorov length scale $\eta=(\nu^3/\varepsilon)^{1/4}$ and velocity scale $u_\eta=(\nu\varepsilon)^{1/4}$. Straight lines indicate k^{-1} and $k^{-3/3}$ behavior.

(provided it is sufficient to ensure a large population of the small eddies), to avoid introducing the domain size as a second outer-layer length scale. This same argument is made in a channel, with its depth setting the streamwise and lateral domains, or in a pipe for domain length. Its only weakness is that the sizing of the domain is based on the arguments *also* used in the similarity theories (resulting in, for instance, the defect law). This makes a verification of the theories faintly circular, much like a validation of the law of the wall that uses fixed values for the grid spacing in wall units (another time-honored policy, which we adopted). These considerations are unavoidable in DNS. In both respects, the concern could be nearly eliminated by adopting extremely safe values for domain size and grid spacing, but that would limit the Reynolds number to a range of little interest.

The time step Δt is set by a maximum Courant–Friedrichs–Lewy (CFL) number of 1.3 anywhere in the domain; this peak occurs near $z^+=10$. In Table I this approach leads to a mild downward drift in wall units, versus Reynolds number. In retrospect, a fixed value could have been applied,

and been more consistent with the grid-spacing policy, provided the stable CFL limit at the highest Reynolds number could be forecast. However, the Δt^+ variation is too small to suspect an appreciable difference in time-discretization errors in the four cases. This code has been run with peak CFL numbers of $\sqrt{3}$ and even 2 without trouble.

II. RESULTS

Mean quantities, indicated by an overbar, are obtained by averaging in space over homogeneous (x,y) planes at each z and in time over at least two full $2\pi/f$ inertial periods [the $Re=2828$ average (over $4\pi/f$) required about 344 000 CPU-processor hours on the p690+ cluster]. In wall scaling at $Re=2828$, this represents about 2.3×10^8 area units and 10^5 time units. The resulting first- and second-order statistics satisfy both components of the mean momentum equation to good accuracy, in that the difference at each elevation between the ageostrophic and stress-divergence terms is typically 10^{-3} to 10^{-4} fG . As a result, the global momentum

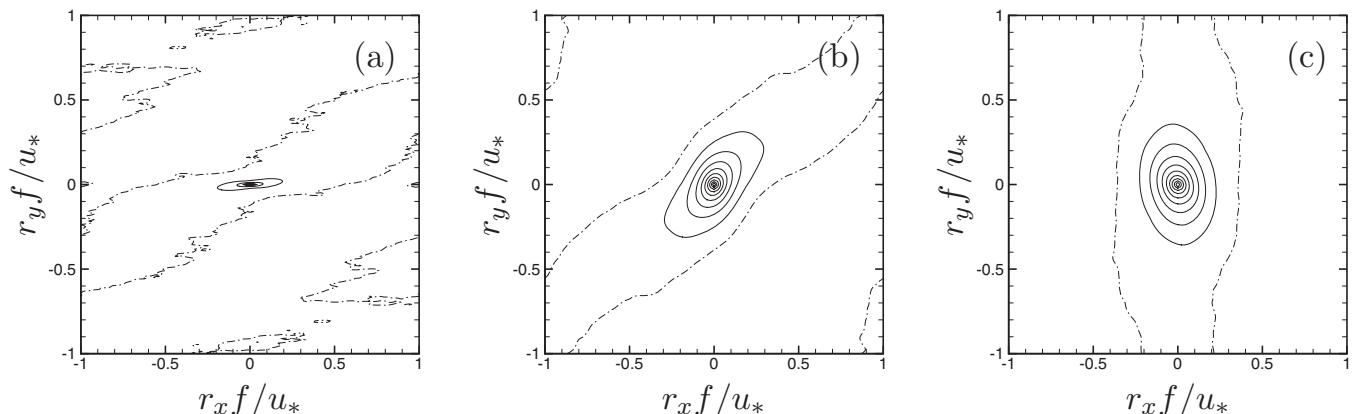


FIG. 3. Contours of horizontal two-point three-component velocity correlation coefficient R_{ii} on planes at (a) $z/\delta^*=0.004(z^+=30)$, (b) $z/\delta^*=0.24(z^+=1866)$, and (c) $z/\delta^*=0.41(z^+=3159)$ for $Re=2828$ DNS: (—) $R_{ii}>0$; (— · —) $R_{ii}=0$; contour interval 0.1. Zero separation at center of plot; maximum (half-domain) separation is $\pm u_* / f$ in both directions.

TABLE II. Time-averaged results.

Source	Re	u_* / G	α_0 (deg)	$u_*^2 / f\nu$	$f\delta_G / u_*$	$f\delta_\tau / u_*$	$1/p_{\text{eff}}^+$
Refs. 1 and 2 (1996)	400	0.06570	27.81	345	0.83	0.65	49
Ref. 1 (1990)	500	0.06270	25.35	491	0.72	0.64	72
Ref. 3 (1999)	1000	0.05390	19.00	1453	0.605	0.60	241
New	1000	0.05350	19.36	1431	0.61	0.605	231
New	1414	0.04971	17.78	2473	0.57	0.58	403
New	2000	0.04668	16.19	4358	0.585	0.58	730
New	2828	0.04367	15.57	7626	0.52	0.55	1241

balance is also quite good: Compared to the exact results of unity and zero (as fractions of u_*^2), the vertically integrated mean momentum equation in the directions orthogonal and parallel to the mean surface shear stress are (in the worse case), respectively, 0.9945 and 0.004. The mean velocity is shown in hodograph form in Fig. 1(b). We observe the expected decrease with Re of the angle α_0 between the surface shear stress and the freestream geostrophic wind \mathbf{G} . A summary of how this and other global parameters vary with Re is given in Table II. (We will return to the question of how well the variation of α_0 and the drag coefficient u_* / G agrees with similarity theory in Sec. II B.) The third result listed, $u_*^2 / f\nu$, is a turbulence Reynolds number, the smooth-wall equivalent of the surface Rossby number (recall that u_* / f is the relevant outer-layer length scale for this flow¹⁰). Two measures of the Ekman-layer depth are also shown in Table II, as fractions of u_* / f . The first, δ_G , is the lowest elevation at which the mean velocity is parallel to the geostrophic freestream \mathbf{G} [i.e., where $\bar{v}=0$; see Fig. 1(b)]. A Reynolds-number dependence is apparent, with $\delta_G f / u_*$ decreasing from over 0.8 to almost 0.5 as Re increases from 400 to 2828. However, some statistical variation is also strongly suggested by its nonmonotonic behavior with Re. This can be attributed to the weak vertical gradient $d\bar{v}/dz$ near the top of the layer [cf. Figs. 10(a) and 24(a) of Ref. 1 or Fig. 3(a) of Ref. 3].

A somewhat more robust measure of the Ekman-layer depth is δ_τ , defined as the height at which the magnitude of the turbulent shear-stress “vector” ($-u'w'$, $-v'w'$) is down to 5% of the surface stress, u_*^2 . The trend in the Re=1000, 1414, 2000, and 2828 values (Table II) of the ratio of δ_τ to u_* / f is also downward, but the Reynolds-number range should be kept in mind. The Reynolds number δ_τ^+ increases by a ratio of 4.84, compared to 5.33 for $u_*^2 / f\nu$; therefore, their rates of growth differ by 6%. It is conceivable that this consistent trend will suggest a refinement to the defect law. In inner-layer units, this corresponds at Re=2828 to $\delta_\tau^+ = \delta_\tau u_* / \nu \approx 4200$, which confirms the relatively large Reynolds number of the present results. The final parameter in Table II quantifies the pressure gradient in the surface shear direction, in terms of inner units. Since the magnitude of the horizontal Ekman pressure gradient $\nabla P / \rho$ (normal to the geostrophic velocity \mathbf{G}) is $|fG|$, the shear-wise component in inner units p_{eff}^+ is $\nu f G \sin \alpha_0 / u_*^3$. The Re=2828 value is $p_{\text{eff}}^+ = 0.00081$, which corresponds to a plane channel flow (for which $p^+ = 1 / \text{Re}_\tau$) at $\text{Re}_\tau = 1241$. A similar measure is the ratio of friction velocity to mean channel centerline velocity: 0.0437.

This skin-friction coefficient $C_f = 0.0038$ will result from a Re_τ of about 1120 (although note that the “negative wake” in the Ekman layer (Fig. 5) tends to depress its effective Reynolds number when comparing with channels and adverse- or zero-pressure-gradient boundary layers). In a flat-plate boundary layer, R_θ would be near 1970 and δ^+ near 900 for the same skin-friction coefficient,⁸ but the Ekman pressure gradient raises the skin friction, thus depressing the analogous Reynolds number obtained this way. The stress-based thickness near 4200 reflects a much longer “tail” than these other measures do; the range of z^+ from 2000 to 5000 is clearly influenced by rotation. This helps place the present DNS in context when comparing to other wall-bounded simulations. The high point of DNS, in the archival literature, has been the channel flow at $\text{Re}_\tau = 2003$.⁴

A. Local quantities

We now examine whether the DNS Reynolds numbers are large enough for statistics to exhibit conclusive similarity. The Re=1000–2828 data are compared in Fig. 4 in outer-layer scaling¹⁰ for velocity and shear stress, in coordinates aligned with the surface shear stress. The collapse is striking, with good agreement of both components of both quantities at least down to $z f / u_* \approx 0.01$, and the normal deviation in the buffer layer, due to the rise of the viscous stress. At the same time, the downward drift with Re discussed over Table II is detectable in the range of $z f / u_*$ between 0.2 and 1.

The inner scaling of the mean velocity at all Reynolds numbers is compared in Fig. 5. Whether the mean velocity at large Reynolds numbers should satisfy a power law^{11,12} or a logarithmic law, and if the latter what exactly the slope $1/\kappa$ and additive constant \mathcal{C} should be,^{13,14} are still a matter of intense debate. As Re increases, the increasingly pronounced logarithmic region appears unmistakable. At first sight, the Re=2828 case has a straight line from $z^+ = 40$ to 1000. However, the fine level of scrutiny which has become the norm in this arena opens up interpretations, unrelated to the mean three dimensionality induced by the Ekman rotation (i.e., not a consequence of the difference between velocity in freestream and in surface shear axes). Recall that the search is for a region that is straight on a semilog plot, and “stretches” as the Reynolds number rises. We are led to detect either regions close to straight (leading to “manual” fits), or inflection points; this has been the norm, but will not

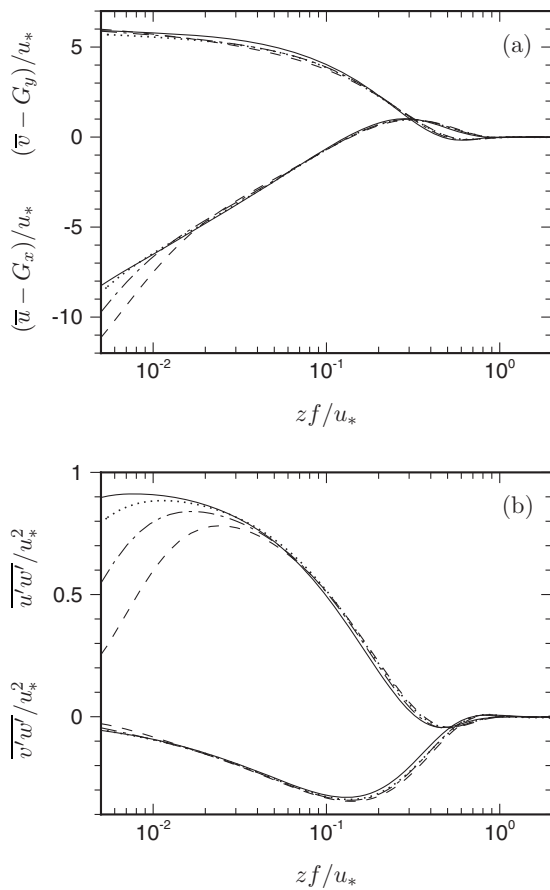


FIG. 4. Outer scaling of (a) mean velocity and (b) Reynolds shear stress, in axes aligned with and orthogonal to surface shear stress: (----) Re=1000; (— · —) Re=1414; (·····) Re=2000; (—) Re=2828.

produce κ with an uncertainty approaching ± 0.01 at DNS-reachable Reynolds numbers. The Karman “constant” has often been sought below $z^+=100$, which is not compatible with the newer conclusions of Österlund *et al.*¹⁴ and Zanoun *et al.*¹⁵ that the region near 70 only contains an inflection

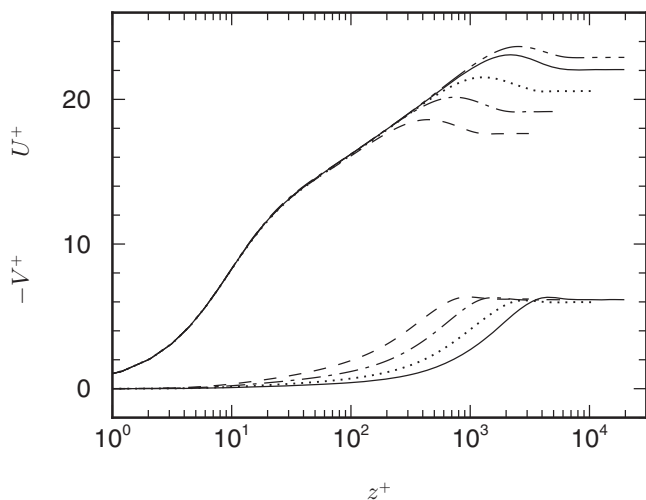


FIG. 5. Inner scaling of mean velocity components aligned with and orthogonal to surface shear stress: (----) Re=1000; (— · —) Re=1414; (·····) Re=2000; (—) Re=2828; (— · · —) velocity magnitude $\sqrt{u'^2 + v'^2}/u_*$ for Re=2828.

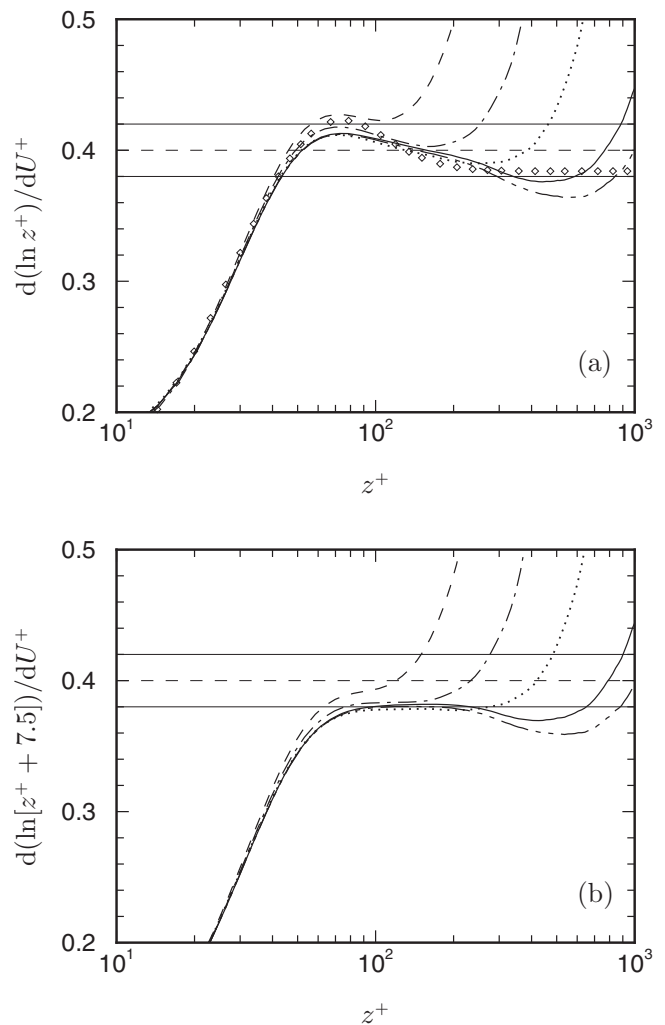


FIG. 6. Karman measures for velocity component aligned with surface shear stress (cf. Fig. 5): (----) Re=1000; (— · —) Re=1414; (·····) Re=2000; (—) Re=2828; (— · · —) velocity magnitude $\sqrt{u'^2 + v'^2}/u_*$ for Re=2828; (\diamond) Chauhan *et al.* (Ref. 16) interpolant.

point, and not a “stretching” layer; in other words, it is a false log layer. In their view the true log layer would begin near 200, with constants (0.38,4.0); the DNS can fit this quite closely, as seen below, but it is not clear the DNS velocity profiles themselves (as opposed to their derivatives, to be seen shortly) would have suggested these values. The one view our DNS results conflict with is that of McKeon *et al.*¹³ and earlier Superpipe papers, in that the profiles do not support a κ value in the 0.42 range, as they found.

A direct measure of the postulated log-law behavior⁸ is given in Fig. 6(a). The term “Karman measure” seems more appropriate to describe $[(z/u_*)(d\bar{u}/dz)]^{-1}$ [or $d(\ln z^+)/dU^+$] than “local Karman constant” or “effective Karman constant.” In a logarithmic layer, this quantity will be constant and equal κ ; also recall that current controversies cover the range [0.38,0.42]. The acceptable smoothness of this quantity, although it is a derivative of that in Fig. 5, and the generally ordered steps with Re of the curves both rule out the possibility of grossly insufficient time sample. The Ekman results gratifyingly collapse for increasing Re, establishing a law of the wall, in contrast with the same rendition of

channel results.^{4,5} On the other hand, the figure disappointingly fails to indicate a log layer to better than ± 0.02 in terms of the Karman measure, even with $\text{Re}=2828$. There is the appearance of a stretching layer, but with a pronounced slope. The trend for the velocity magnitude to produce a lower value of κ than the wall-aligned velocity does, beyond $z^+=300$ for $\text{Re}=2828$, is confirmed, but is minor relative to the slope. Hu *et al.* do not show the Karman measure, but we extracted it from the database they make available, and it is close to that shown by Hoyas and Jiménez, in that the slope is Reynolds-number dependent starting near $z^+=90$. The latter authors doubt the “relevance” of the measure used here and in their paper, and move on to other aspects of the turbulence. However, DNS having secured a full order of magnitude in Reynolds number over the first channel study and therefore over values which can sustain turbulence, we find the conflict with theory worth defining and discussing, as follows.

Channel flow failed to return a collapse of the Karman measure beyond $z^+ \approx 100$. The agreement between independent simulations is too good to suspect a flaw in them. The Ekman flow has the collapse to noticeably higher z^+ , but fails to return a plateau, and at first sight suggests that the Karman measure will dip to very low values in the outer region at Reynolds numbers not reached here. However, the true trend is not clear. The Karman measure has a local minimum in that region (at $z^+=103$ for $\text{Re}=1000$) which is representative of its trend. Its values at the four Reynolds numbers are 0.423, 0.403, 0.390, and 0.376; the decrease may be slowing, whereas a straight-line behavior in logarithmic axes would give constant increments for a geometric series in Re . Statistical convergence is slow in this region.

Figure 6(a) then suggests the following tentative interpretation. Logarithmic behavior of the velocity results from inviscid blocking of motion by the wall. This is modified near the wall by viscous effects, which reign in a buffer layer of thickness a few tens of wall units. These effects fully control the log-law intercept C . If so, it is natural to postulate a virtual origin not only for velocity but also for height. Virtual origins are ubiquitous in rigorous higher-order theories, such as boundary-layer theory, which introduces the displacement thickness. Unfortunately here, this has the nature of a conjecture rather than a mathematical fact, because we do not have access to a “governing equation.” Nevertheless the outcome is more than intriguing as seen in Fig. 6(b), in which a shift by $a^+=7.5$ wall units is introduced. The stretching layer is now horizontal, within the statistical scatter, with a range of approximately [100,300] at the highest Re . The best fit is slightly below 0.38, discarding the 3D effects. This is our first key figure.

The arguments against this presentation are that it would be cosmetic, and that a version of Fig. 6(a) with sufficient Reynolds number must also asymptote to the same κ value. This is correct. Yet, it is plausible that allowing for a shift provides access to the true value of κ at a lower value of Re . A further argument arises from the empirical fit to boundary-layer experiments, given by Chauhan *et al.*¹⁶ and shown in Fig. 6(a). Their Karman measure *very* similarly to ours although 0.01 higher, but drops toward its asymptote more

steeply. Their analytical a^+ is only 1.5, and, in fact, is only a secondary feature of a Padé fit they created and which favors the lower region. With a shift by 7.5, their results would overshoot, and then undershoot. We have to conclude that experiment and DNS agree on the general shape of the Karman measure and on the most likely value of the Karman constant, but that this level of derivative is high enough to bring out a quantitative difference. Yet, the integral below their function and our profiles (in the axes of Fig. 6) has cancellations between the region near 70 and that near 200, with the result that the velocity U^+ itself agrees to plotting accuracy up to about 400. This is a very positive development, although again there is no explanation for even slightly different behavior in channels.

B. Global Ekman-layer scaling

Throughout the course of our Ekman-layer studies^{1,3} we have tested similarity theory⁷ for which the existence of an overlap layer is central in order to extend the DNS results to arbitrary Re , pending good agreement in the Re range covered. Even if one accepts the validity of the log-law relationship (which we are inclined to do), it must be admitted that this procedure is now less straightforward than previously, due to the current uncertainty regarding the exact values of κ and C , possible a^+ shifts, and the exact z^+ location above which they are declared valid. In engineering boundary layers, the variation of the skin-friction coefficient with Reynolds numbers has emerged as a more impartial tool to determine κ than fits to velocity profiles, and this is what the exercise shown here amounts to. Conversely, it requires a wide Reynolds-number range.

The postulated Ekman-layer similarity relationships derive from matching asymptotic expansions ruled by simple (although nontrivial) assumptions on inner and outer scaling of the velocity profile, namely, the law of the wall and the defect law:

$$\kappa \frac{G}{u_*} \cos \theta - \ln \left(\frac{u_*^2}{f\nu} + a^+ \right) = -\mathcal{A}, \quad (1a)$$

$$\kappa \frac{G}{u_*} \sin \theta = \mathcal{B}, \quad (1b)$$

where

$$\theta = \alpha_0 + \left[C_5 - \frac{a^+}{\kappa} \left(\ln \left(\frac{a^+ f\nu}{u_*^2} \right) + C' \kappa - 1 \right) \right] \frac{f\nu}{u_*^2}. \quad (2)$$

These equations come from replacing Eq. (15) in Ref. 17 with $\hat{U}^+ - e^{-i\phi^*} Z = f_1(y^- + a^+/R_l) + f_5(y^+)$ (in that article's notation). Here, C' is the intercept of the (Ekman) log law in outer units, seen in Fig. 4(a) to be about 5.4. This agrees with the equation $C' = C + \mathcal{A}/\kappa$, with the value of \mathcal{A} which is determined empirically below. Also, C_5 is a universal constant tied to the law of the wall, defined as $\int_0^+ f_5 dz^+$, with $f_5(z^+) = \bar{u} - [(1/\kappa) \ln(z^+ + a^+) + C]$, and z_{\log}^+ any location inside the log layer (above which $f_5 \equiv 0$). \mathcal{A} and \mathcal{B} are similarity coefficients of the Ekman layer, i.e., they are not universal to wall-bounded flows. The correction to Eq. (1a) due to the shift is,

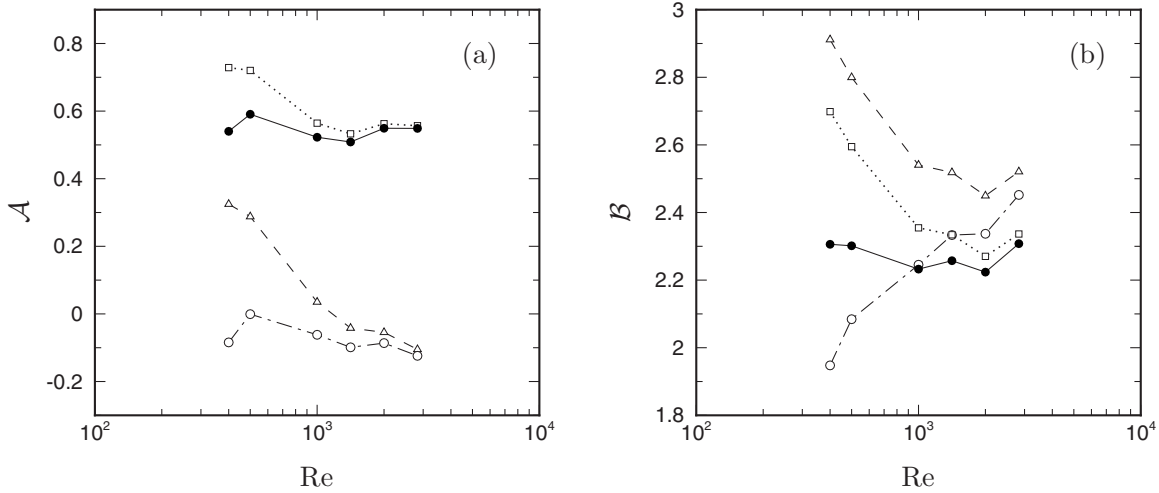


FIG. 7. Test of similarity theory for various combinations of κ , a^+ , C' , and C_5 : (Δ --- Δ) (κ, a^+, C', C_5)=(0.41,0,0,0); (\circ — \circ) (0.41,0,0,-58); (\square ···· \square) (0.38,0,0,0); (\bullet — \bullet) (0.38,7.5,5.4,-88). Coefficients \mathcal{A} and \mathcal{B} in (a) and (b), respectively, given by Eqs. (1a) and (1b).

to leading order, $a^+ f \nu / u_*^2$. This is only about 0.02 even at $Re=400$ and is small relative to the trends and scatter in \mathcal{A} .

The higher-order correction of Spalart,¹⁷ which consists in the difference between θ and α_0 in Eq. (2), is needed at the low Re typical of early DNS work. The constant C_5 , assumed in Refs. 1, 3, and 8 to fall between -64 and -52 (without any a^+ shift), has been extremely sensitive to uncertainty of the additive log-law constant and the location $z_{\log}^+|_{\min}$ above which $f_5 \equiv 0$: A very modest variation of ± 0.1 in C_5 produces a change in $\pm 0.1 z_{\log}^+|_{\min}$, which if $z_{\log}^+|_{\min} = 200$ (cf. Fig. 6), corresponds to ± 20 . However, the tight fit of the present profiles to the proposed log law in Fig. 6(b) has improved this situation, if the value of a^+ is accepted. The present results indicate that $C_5 \approx -88$, from the profile in Fig. 5. The basic, classical theory of Csanady⁷ and Blackadar and Tennekes¹⁰ omits C_5 and a^+ , so that $\theta = \alpha_0$ instead of Eq. (2). The generalized and basic theories converge if Re is greater than about 3000; see Fig. 22(b) of Ref. 1 and Fig. 8 below.

These equations contain six empirical constants, of which κ , a^+ , and C_5 are not limited to the Ekman layer. These three can therefore be *tested* by reverse-calculating \mathcal{A} and \mathcal{B} from Eq. (1), and observing whether the results are indeed constants [C' multiplies a small correction, and is taken from Fig. 4(a) with sufficient accuracy]. Equation (1a) sets the decay of the skin-friction coefficient with Reynolds number and has the advantage of involving \mathcal{C} only weakly (through C_5 , which enters θ); its analog is used routinely in the flat-plate boundary layer. The result of this exercise is shown in Fig. 7, in which a traditional value $\kappa=0.41$ and the one suggested by the DNS Karman measure, 0.38, are candidates. Equation (1b) is much more sensitive to C_5 . The scatter between cases is appreciable, but not large enough to hide the overall trends (there could be reason to discard the 400 case as an “outlier,” possibly based on strong “low-Reynolds-number effects,” or to average it with 500). In particular, the residual slope in \mathcal{A} and especially in \mathcal{B} is definitely stronger with $\kappa=0.41$ than with $\kappa=0.38$, confirming the Karman measure findings. This is our second key figure.

A similar approach to the channel, using the centerline

velocity and a log law without shift, yields the following three values for κ between the four cases of Hoyas and Jiménez: 0.399, 0.370, and 0.406. The scatter is too large to suggest any kind of a high-Reynolds-number asymptote.

The level of success of the theory for both the basic⁷ and generalized¹⁷ versions of Eq. (1) with $\kappa=0.38$ is measured in a slightly different manner in Fig. 8. This involves defining \mathcal{A} and \mathcal{B} as the average of the values given by u_* / G and α_0 at $Re=2000$ and 2828. With these choices, the similarity coefficients \mathcal{A} and \mathcal{B} for the generalized theory are $(\mathcal{A}, \mathcal{B}) = (0.56, 2.32)$, with $a^+=7.5$, $C'=5.4$, and $C_5=-88$; the corresponding values for the basic theory are $(\mathcal{A}, \mathcal{B}) = (0.56, 2.30)$. The small difference between the two sets indicates that $Re=2828$ is indeed close to the maximum Re at which the low- Re correction is material. (At $Re=2828$, the higher-order correction $\alpha_0 - \theta$ is less than a quarter of a degree.) Especially noteworthy is the ability of both basic and low- Re versions to capture the variation of u_* / G over the full $400 \leq Re \leq 2828$ range, and of the generalized theory to predict α_0 . The level, slope *and* curvature of *two* curves are obtained with only three Ekman-specific disposable constants.

III. CLOSING REMARKS

The Reynolds number of the present DNS is large enough to enter debates over the scaling laws with little of the arbitrariness associated with choosing a range over which to curve fit the velocity. Extracting a Karman constant from the velocity derivative has proven to be a severe test and DNS, even in recent channel studies at comparable Reynolds numbers, has been unable to propose a value (discounting the inflection point with Karman measure near 0.43 near $z^+ = 70$). The present results are more encouraging. They give a definite trend toward low values of κ , in agreement with modern boundary-layer experiments, but not pipe experiments. Fully developed pipe-flow DNS is sorely lacking. It is to be hoped for the sake of turbulence theory that proposals

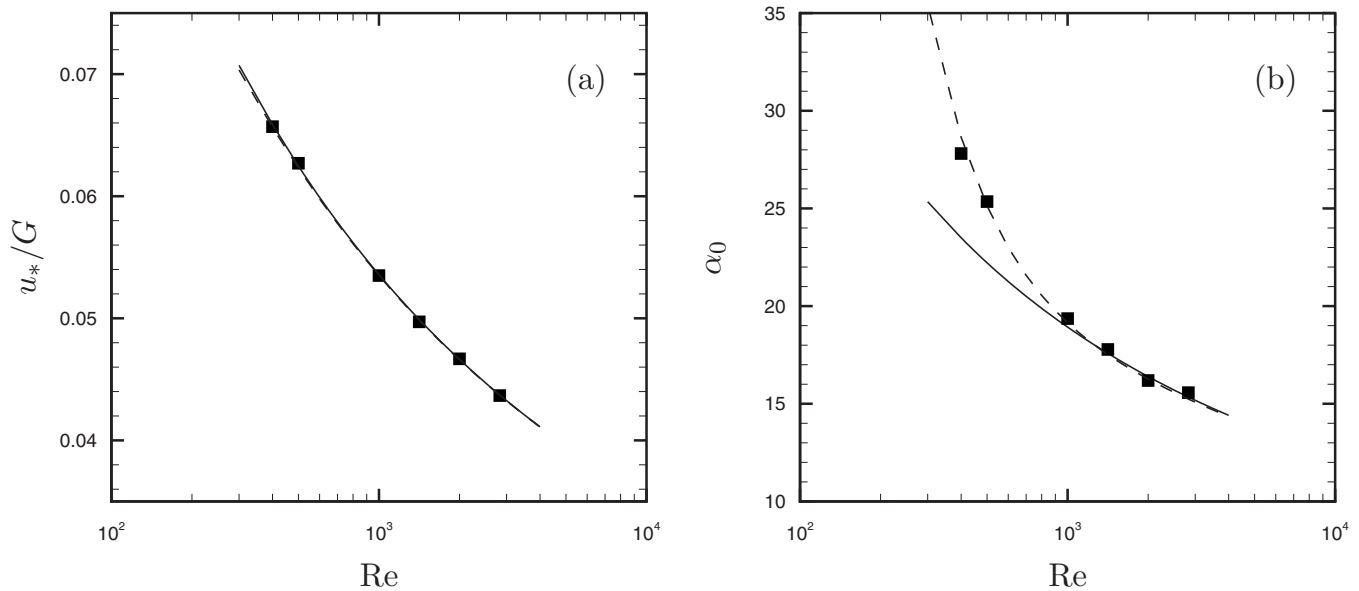


FIG. 8. Comparison of basic and generalized similarity theory, and DNS results for $\Omega_H=0$ for (a) geostrophic drag coefficient u_* / G and (b) surface shear angle α_0 : (—) basic theory (Ref. 7) with $\mathcal{A}=0.56$, $\mathcal{B}=2.30$, and $\kappa=0.38$; (---) generalized theory Ref. 17) with $\mathcal{A}=0.56$, $\mathcal{B}=2.32$, $\kappa=0.38$, $C'=5.4$, $a^+=7.5$, and $C_5=-88$. Symbols indicate DNS results.

of different values for κ in different flows will lose out. Independent boundary-layer DNS is also very desirable.

The interpretation is cautious for two reasons. The first is that the κ values are well outside what was the accepted range. The engineering impact is surprisingly small, however. The Karman constant primarily controls the variation of the skin-friction coefficient with Reynolds number and even at large-airplane values, the effect of switching from 0.41 to 0.38 is only of the order of 2%. The value 0.38 is, in fact, close to an empirical correlation used by Boeing since the 1960s. Also note that the log law we are proposing gives $U^+=16.21$ at $z^+=100$, which is very close to the consensus value of 16.24 in the collaborative testing of turbulence models. Visible differences in U^+ due to a switch from 0.41 to 0.38 only begin around $z^+=2000$.

The second reason for caution is that the most favorable view of the log law comes when the vertical coordinate is shifted by the amount $a^+=7.5$. Having an additional adjustable constant makes the existence of a plateau less compelling, the more so because the plateau level, here 0.38, is not known independently except for the experimental evidence (compare this with finding a plateau at $-\frac{5}{3}$ in a Kolmogorov situation). Such shifts are of course present in older empirical laws, starting with that of Reichardt which has a shift by $a^+=1/\kappa$ due to the molecular viscosity, but more meaningfully with Squire¹⁸ in 1948 and $a^+=-5.3$. Yet, the value 7.5 is of the same magnitude, but opposite sign. His physical reasoning is not unlike ours, but is aimed at the buffer layer, much like van Driest's damping. Values as low as -8 have been advocated, showing a grave lack of consensus [since the Karman measure is, to leading order, $\kappa(1+a^+/z^+)$, a high value of κ can be offset locally by a low value of a^+]. None of the classical papers entertained the likelihood of the velocity profile mildly overshooting the log law (thus making a^+ positive, driven by the behavior well above $z^+=100$ in-

stead of the buffer layer), but DNS and some experiments now strongly agree on this. Mathematically, the idea that the Karman measure would approach a constant value with a difference of order $1/z^+$ is plausible, but emphatically is not provable. Unfortunately in physical terms, viscous effects have normally yielded positive offsets, i.e., the displacement thickness is positive. A simple model of a Hiemenz region under a "splating" event yields an offset of the order of $+5$ wall units, rather than -7.5 : The use of $\ln(z^++7.5)$ places the virtual origin below the wall. However, the shift has no effect on the first finding of this study, which concerns the gradual establishment of the law of the wall, a weaker property than the log law. The difference with channel DNS results is meaningful. Also, the shift can be viewed as cosmetic, and when examined in detail, is not in precise quantitative agreement with experiments. On the other hand, these are recent boundary-layer experiments, which do not agree with older knowledge or recent pipe experiments either. The scene is fairly fluid.

To be complete, we recall that the a^+ shift is viewed as universal and a permanent feature of the law of the wall, just like the Karman constant, and *not* a function of the flow Reynolds number; this is not a "higher-order log law" (in our view, none of the proposals of this type have been compelling). Finally, the shift primarily addresses the behavior in the z^+ range of $[100,300]$, so that a shift by 7.5 represents only a few percent of the wall distance in question; correspondingly, the change in U^+ between $z^+=100$ and $z^+\gg 100$ is only 0.19. Omitting the shift by 7.5 altogether alters U^+ at $z^+=300$ by only 0.07.

Were the shift to become accepted, the value of a^+ proposed should be considered to have an uncertainty of at least ± 1 , the adjustment to Ekman-layer profiles in Fig. 6 leaving a little room. If κ is set to 0.38 and a^+ to 7.5, the intercept C

is about 3.9. To summarize, the logarithmic law we are proposing is

$$U^+ = \frac{1}{0.38} \ln(z^+ + 7.5) + 3.9.$$

ACKNOWLEDGMENTS

This work was done as part of the UK Turbulence Consortium, sponsored by the Engineering and Physical Sciences Research Council (Grant No. EP/D044073/1). Computations were made on the U.K./EPSRC HPCx system. Thanks are due to Dr. Mike Ashworth of CCLRC Daresbury Laboratory, for converting the DNS code into its present FORTRAN format. An abbreviated version of this paper was presented at the ERCOFTAC Direct and Large-Eddy Simulation-6 Workshop in Poitiers.

¹G. Coleman, J. Ferziger, and P. Spalart, "A numerical study of the turbulent Ekman layer," *J. Fluid Mech.* **213**, 313 (1990).

²The Re=400 case considered here is an unpublished larger-domain version of Case A90 from Ref. 1. While measurable, the differences in global statistics between the small- and large-domain simulations are within the quoted uncertainty of the earlier data.

³G. Coleman, "Similarity statistics from a direct numerical simulation of the neutrally stratified planetary boundary layer," *J. Atmos. Sci.* **56**, 891 (1999).

⁴S. Hoyas and J. Jiménez, "Scaling of the velocity fluctuations in turbulent channels up to Re_τ=2003," *Phys. Fluids* **18**, 011702 (2006).

⁵Z. Hu, C. Morfey, and N. Sandham, "Wall pressure and shear stress spectra from direct simulations of channel flow," *AIAA J.* **44**, 1541 (2006).

⁶P. Spalart, R. Moser, and M. Rogers, "Spectral methods for the Navier-Stokes equations with one infinite and two periodic directions," *J. Comput. Phys.* **96**, 297 (1991).

⁷G. Csanady, "On the 'resistance law' of a turbulent Ekman layer," *J. Atmos. Sci.* **24**, 467 (1967).

⁸P. Spalart, "Direct simulation of a turbulent boundary layer up to $R_\theta = 1410$," *J. Fluid Mech.* **187**, 61 (1988).

⁹The earlier Re=1000 run used $\ell_z = 0.23u_* / f$, despite the erroneous claim in Ref. 3 that $\ell_z = 0.23D$.

¹⁰A. Blackadar and H. Tennekes, "Asymptotic similarity in neutral barotropic planetary boundary layers," *J. Atmos. Sci.* **25**, 1015 (1968).

¹¹G. Barenblatt, "Scaling laws for fully developed turbulent shear flows: Part I. Basic hypothesis and analysis," *J. Fluid Mech.* **248**, 513 (1993).

¹²M. Wosnik, L. Castillo, and W. George, "A theory for turbulent pipe and channel flows," *J. Fluid Mech.* **421**, 115 (2000).

¹³B. McKeon, J. Li, W. Jiang, J. Morrison, and A. Smits, "Further observations of the mean velocity distribution in fully developed pipe flow," *J. Fluid Mech.* **501**, 135 (2004).

¹⁴J. Österlund, A. Johansson, H. Nagib, and M. Hites, "A note on the overlap region in turbulent boundary layers," *Phys. Fluids* **12**, 1 (2000).

¹⁵E. Zanon, F. Durst, and H. Nagib, "Response to 'Comment on "Evaluating the law of the wall in two-dimensional fully developed turbulent channel flows"'", *Phys. Fluids* **16**, 3509 (2004).

¹⁶K. A. Chauhan, H. M. Nagib, and P. Monkewitz, "On the composite logarithmic profile in zero pressure gradient turbulent boundary layers," AIAA Paper No. 2007-532, 2007.

¹⁷P. Spalart, "Theoretical and numerical study of a three-dimensional turbulent boundary layer," *J. Fluid Mech.* **205**, 319 (1989).

¹⁸H. Squire, "Reconsideration of the theory of free turbulence," *Philos. Mag.* **39**, 1 (1948).